In Situ Root Volume Estimation Using Ground Penetrating Radar

Janet E. Simms, S. Kyle McKay, Robert W. McComas and J. Craig Fischenich
U.S. Army Engineer Research and Development Center, 3909 Halls Ferry Road, Vicksburg, MS 39180
Email: Janet.e.simms@usace.army.mil

ABSTRACT

A ground penetrating radar (GPR) and root excavation study were conducted to determine the efficacy of GPR for estimating subsurface tree root volume. The survey was conducted in sandy soil, which is favorable for GPR imaging. The tree was a loblolly pine (*Pinus taeda*) that was isolated from other trees to minimize outside influences. GPR antenna frequencies of 450 MHz, 900 MHz, and 1200 MHz were used to map subsurface profiles over a 9-m^2 sample grid, and six 1-m^2 cells of the root system were subsequently excavated to a depth of 1 m for verification. The 900 MHz GPR was successful at mapping the larger tree roots (>2 cm) and some smaller roots (<2 cm). A simple approach based on average signal strength was used to estimate root volume from the GPR data. The total root volume estimate based on the GPR data compared well with the total root volume determined from the in situ measurements when information from all of the excavated cells was used (<2% error). However, accuracy reduced significantly (30% error) when only three verification cells were used, representing near, intermediate, and far distances from the tree. Matching the GPR root volume to a particular in situ root volume did not improve the root volume estimation.

Introduction

Tree roots influence a variety of ecological processes (Day *et al*., 2010; Guo *et al*., 2013a, 2013b) on a global scale (*e.g*., carbon storage) and local scale (*e.g*., soil erosion control, increase water infiltration, improve soil biological activity), but their proximity to infrastructure, such as buildings, roads, levees, walkways, and pipes, can cause or initiate multiple types of structural problems. Instances of tree roots penetrating infrastructure have been documented where older or poorly constructed sewer systems exhibited higher rates of root intrusion (Randrup *et al*., 2001) and fibrous roots of a sycamore maple (*Acer pseudoplatanus*) penetrated the mortar joints of an underground utility room (Schroeder, 2005). Corcoran *et al*. (2011) studied the influence of woody vegetation roots on earthen levees, concluding that they can be either beneficial or detrimental depending on regional location, position of the tree on the levee, soil type, soil moisture, local climatic conditions (precipitation, wind, temperature, etc.), and tree properties (species, root strength, root architecture, height, age, etc.). Thus, knowledge of tree root location and the subsurface volume that they encompass can be useful in assessing trade-offs associated with infrastructure and environmental management decisions. Non-destructive root mapping is desirable because the excavation of roots is damaging to the tree, possibly damaging to a structure, time consuming and costly.

Over the past 15 years, ground penetrating radar (GPR) has been used to detect and map tree roots to estimate diameter, architecture, and biomass. Guo *et al*. (2013a) provide a concise review of GPR use for coarse root detection and quantification. The majority of studies have been conducted in sandy soils because its electrical properties are conducive to GPR surveying. Relative to other subsurface targets, tree roots are generally smaller, have a lower soil–target relative dielectric permittivity contrast than other common GPR targets (*i.e*., metals, voids, saturated soils), and have a less structured design. Because of these factors, soil clutter (any target that is not the desired target) can interfere with or mask the detection of tree roots, rendering GPR ineffective. Even in a relatively homogeneous soil, the addition of small amounts of clay, especially when combined with moderate to high moisture content, will attenuate the GPR signal, thus reducing the depth of investigation and ability to detect roots. Existing work has shown that under favorable

 DOI: #10.2113/JEEG22.3.209

soil moisture and texture conditions, *i.e*., moist, sandy soils, GPR can effectively identify known roots (Butnor *et al*., 2001; Barton and Montagu, 2004; Hirano *et al*., 2009; Yokota *et al*., 2011; Zanetti *et al*., 2011; Guo *et al*., 2013a; Guo *et al*., 2013b; Freeland, 2015; Yeung *et al*., 2016), and some success has been achieved in estimating root volume and biomass (Butnor *et al*., 2008; Cui *et al*., 2013; Danjon *et al*., 2013; Zhu *et al*., 2014). A few studies have attempted to measure root architecture in situ with GPR (Hruska *et al*., 1999; Stokes *et al*., 2002; Cermak *et al*., 2006; Danjon and Reubens, 2008; Freeland, 2015) and have shown that the effectiveness of GPR increases when coupled with invasive sampling with cores, pits, or trenches (Butnor *et al*., 2003; Nadezhdina and Cermak, 2003).

It is necessary to distinguish root volume from root ball volume when using geophysical techniques for their detection. Root volume relates to the individual roots, whereas root ball volume considers the primary root mass as a single entity. In situations where individual roots cannot be distinguished with GPR, it may still be possible to differentiate the root ball volume. Corcoran *et al*. (2011) performed GPR and electrical resistivity surveys encompassing individual trees in different soil types. They found that in instances where individual tree roots could not be distinguished, the general extent of the root ball volume could be identified. The root ball volume exhibited either a higher or lower electrical conductivity depending on the background soil, and higher dielectric permittivity than the surrounding soil. Even in a clay soil, the GPR response proximal to the tree was notably different from the response beyond the primary root structure.

Different approaches have been used to estimate root volume based on GPR data. Such methods include direct methods involving the use of a reflection strength threshold or index (Butnor *et al*., 2008; Cui *et al*., 2013; Zhu *et al*., 2014), and indirect methods that use root diameter determinations to estimate root volume (Cui *et al*., 2011). Butnor *et al*. (2001, 2003) have had limited success in correlating GPR signal strength with root diameter because of influences such as signal attenuation with depth, oblique angle crossing, and dielectric properties of the medium. Barton and Montagu (2004) found a correlation between waveform zero crossings with root diameter; however, it was only applicable to the 500 MHz data and not to the 800 MHz or 1,000 MHz data.

The objective of this study is to examine GPR efficacy for in situ measurement of root location and volume estimation under favorable instrument conditions. To do so, we collected 9 m^2 of high-resolution GPR data around a loblolly pine (*Pinus taeda*), excavated six 1-m^3 sub-samples from this zone, and measured three-dimensional (3-D) root locations with an electromagnetic digitizer. The volume estimations from the GPR data were then verified relative to the in situ excavation measurements. Because GPR response is highly dependent on subsurface conditions, we chose to use a simplistic direct method based on signal amplitude strength relative to background and applying a linear fit to the data. This approach can be used at any site where an optimal signal threshold value is selected for the given data set.

Study Site

The study site is located at a gravel mining operation in Vicksburg, MS. The site contains a lone loblolly pine (*Pinus taeda*) situated on top of a large man-made pile of sand spoil from the mine. The sand was stockpiled from a 3.1- to 12.2-m thick layer of naturally occurring coarse sands and gravels (Corcoran *et al*., 2011) and is well sorted and classified as a gravelly sand (SW). The gravel in the sand was previously washed and concentrated to primarily a pea gravel size with approximately 10 to 15% volume. This particular loblolly pine was chosen because it is isolated from neighboring trees by more than 10 m. The tree has an estimated height of 8.8 m, canopy width 10.4 m north–south (N–S) by 8.8 m east–west (E–W), and diameter at breast height of 40 cm. The mean annual temperature and rainfall at the site are 18.6°C and 147.3 cm, respectively. One week following the GPR data collection, soil moisture content measurements were acquired using an Aquaterr M-300 meter. Measurements were taken at the center of each of the nine grid cells. The average volumetric moisture contents at depths of 10, 20, 30, 40, and 50 cm were 23.1, 24.7, 26.4, 31.4 and 33%, respectively.

A 3-m×3-m sampling grid oriented N23E was established on the east side of the tree as a consistent spatial reference for subsequent analyses (Fig. 1). The western edge of the grid was 0.5 m east of the base of the tree. String was stretched across the grid at 1-m intervals to demarcate the boundaries used for the in situ root sampling. For the GPR survey, string lines were spaced at smaller intervals and used as survey paths to facilitate data acquisition. The nine sampling cells were designated by a letter and number for reference purposes. The ground surface had very little surface vegetation.

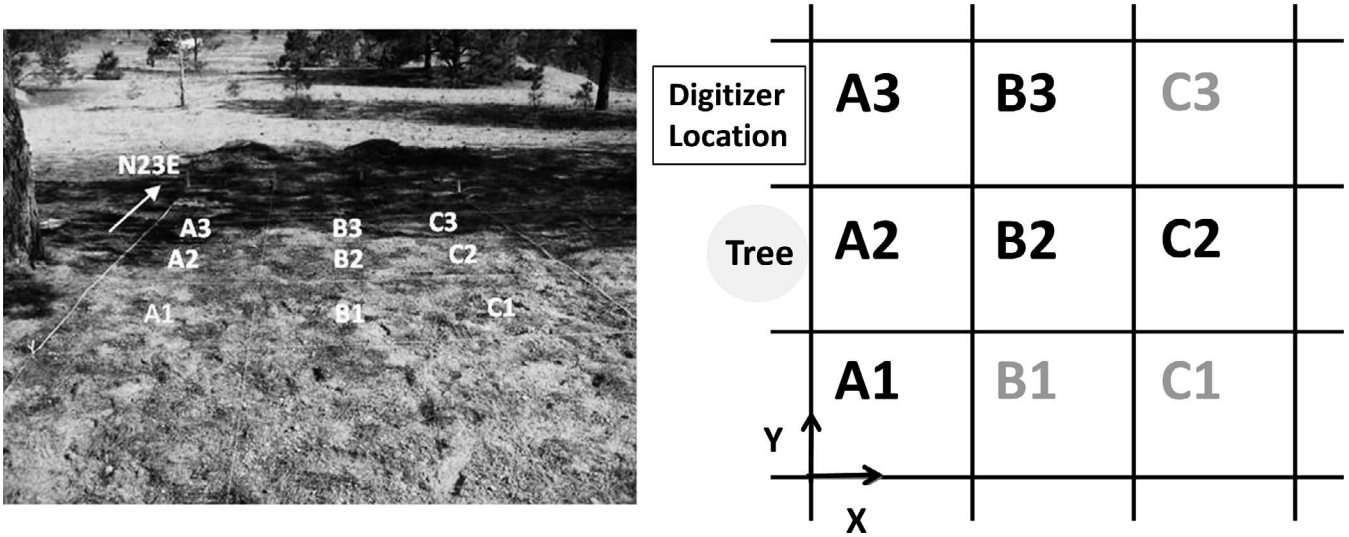

Figure 1. (left) Photograph of the survey area with grid cells overlaid and (right) schematic of the 3-m×3-m grid showing the tree and digitizer locations. The cells with bold labels were excavated.

Methods

Ground Penetrating Radar

The GPR survey was performed to map the subsurface location of roots extending from the study tree and to use the data to estimate the root volume. The GPR survey was conducted after a heavy rain the previous night. The sand is considered clean and well drained, so the precipitation did not appear to inhibit the radar survey. The GPR survey used a Sensors & Software, Inc. (S&S) pulseEKKO 1000 high-frequency system. Three antenna frequencies were used: 450 MHz, 900 MHz, and 1200 MHz. Data were collected in the N–S direction with the 450 and 1200 MHz antenna, and in both the N–S and E–W directions with the 900 MHz antenna. We were unable to acquire data in the E–W direction for all antennae because of time and cost constraints. Although the 1200 MHz antenna provides higher resolution, we opted to use the 900 MHz antenna for the orthogonal data set because it provided greater depth of interrogation. The antennae were oriented perpendicular to the survey line for all data collects. A wheel odometer was used to track distance traveled, with a 2-cm along-line step increment used with the 450 MHz antenna and a 1-cm step with the 900 and 1200 MHz antennas. Survey line spacing for the 450 and 900 MHz antennas was 25 cm, whereas a 10-cm line spacing was used with the 1200 MHz antenna.

The GPR data were processed, visualized, and exported using S&S EKKO_Project (V2R2) and EKKO_Mapper (V4R1). The E–W and N–S data sets were merged and then processed. Standard processing steps were followed, including signal saturation correction (DEWOW, a high-pass filter that compensates for a slowly decaying low frequency transient on the trace), background subtraction, spreading and exponential calibrated compensation (SEC) gain (compensates for weaker signals at depth by ramping the gain between a start and maximum gain value), and migration. An electromagnetic wave velocity of 0.133 m/ns was determined through hyperbola fitting. The gridded data were exported as a 3-D file in hierarchical data format (HDF) for import to Golden Software's Voxler (V3.3) processing and visualization software. Each point within the exported grid is represented by the average signal strength (amplitude) at that point. A slice resolution (pixel), which controls the x- and y-grid dimensions, of 2 cm was used, along with a thickness value, which controls the z-grid dimension, of 2.8 cm. Within Voxler, the grid volume can be processed as an entire volume or smaller units. For this effort, computations were done on the entire grid, multiple 1-m cubes (representing the excavated cells), and individual 1-m cubes. An isosurface was generated for each volume unit based on a single isovalue chosen for the entire grid that provided a realistic representation of the mapped tree roots. An isosurface volume was calculated that represents the volume equal to and greater than the chosen isovalue. This assumes that any response equal to or greater than the chosen isovalue was caused by a tree root. Calculated GPR isosurface volumes were compared with the in situ root volume estimated from the root digitization.

In Situ Root Measurement

To verify GPR predictions, six of the nine 1-m^2 cells were excavated and roots were measured in situ. Ideally, all nine cells would have been excavated. However, a limited data collection window along with funding constraints prohibited complete excavation of the study plot. The sub-sampling method was also originally intended to provide local calibration for the GPR. For instance, a study team could collect GPR data over an entire root zone (or stand), and excavate only a few random cells for local calibration. Thus, complete excavation of the study plot was not the explicit objective of our field investigation. GPR was expected to detect roots no smaller than 2-cm diameter (Hirano *et al*., 2009); thus, verification cells were selected to maximize root size (Fig. 1). Each 1-m^2 cell was excavated in 25-cm increments to a depth of 1 m to capture changes in root properties as a function of depth. Soil was removed using a GuardAir Air-Spade 2000 with a 6.4 m^3/min (225 ft^3/min) nozzle supplied by a 10.6 m^3/min (375 ft^3/min) air compressor (see Danjon and Reubens (2008) for a review of root architectural methods). This technique has been shown to produce minimal disturbance to small roots, with roots as small as 1 to 2 mm remaining after excavation (Cermak *et al*., 2006; Danjon *et al*., 2008). For each depth increment, a representative soil sample was taken for analysis of grain size, gravimetric soil moisture on the excavation date, and total organic content.

Following excavation of each 25-cm layer, roots less than 2-cm diameter were clipped and reserved for laboratory analysis. Remaining coarse roots were labeled and marked for digitization, and the diameter was measured with a Vernier caliper at each digitization point. Digitization points were taken at 5-cm intervals along a given root unless changes in root diameter, shape, or orientation required smaller intervals (Di Iorio *et al*., 2005). Root position was measured along the top of the root with a 3-D digitizer (3SPACE Fastrak, Polhemus, Long Ranger Option) using low-frequency electromagnetic field sensing and driven by Polhemus software (FTGui). Root digitizations were used to calculate root length and, assuming roots are cylindrical between digitization points, the length was combined with measurements of diameter to estimate coarse root volume. Numerous local benchmarks were established to verify instrument stability prior to and following a root measurement. Benchmarks were also used to assess precision of the digitizer by surveying each benchmark a minimum of 60 times, which indicated that the standard deviation of measurements at the maximum root extent was less than 0.25 cm.

Laboratory Analyses

Soil samples (24 samples total) from four depth ranges (0–25 cm, 25–50 cm, 50–75 cm, and 75–100 cm) in each excavated grid cell were sealed and returned to the laboratory. The samples were weighed, oven dried at 180°C for 24 hours, and reweighed to determine gravimetric moisture content. The samples were then subjected to grain size analysis by mechanical sieving. Total organic content (TOC) was determined for each soil sample by drying three sub-samples at 550°C for 1.5 hours.

Clipped roots (*i.e*., those < 2 cm) were oven dried at 180°C for 24 hours to determine organic dry mass. The clipped root volume was measured for all root samples greater than 100 g by measuring the change in volume in a graduated cylinder after submerging the roots. The density of each clipped root sample was then calculated using the mass and volume measurements.

Results

Ground Penetrating Radar

The moist sand on the sample date and lack of subsurface targets other than the tree roots provided a good medium for GPR signal propagation. Example radar profiles acquired using each frequency are shown in Fig. 2. Based on a subsurface electromagnetic wave velocity of 0.133 m/ns, the depths of investigation were about 0.9 m, 1.6 m, and 2.0 m for the 1200 MHz, 900 MHz, and 450 MHz antenna frequencies, respectively. Figure 3 presents a comparison of a depth slice image at a comparable depth range for the three antenna frequencies. This figure illustrates how resolution improves as the frequency of the antenna increases. As stated previously, data were acquired in the N–S direction only with the 450 and 1200 MHz antennas, while data were collected in both the N–S and E–W directions with the 900 MHz antenna. Figure 4 demonstrates the improvement in root delineation achieved by using a combined orthogonal data set as opposed to a data set acquired in a single direction. This is because the GPR response is strongest when the long axis of a target is oriented perpendicular to the direction the antenna travels. Observe in Fig. 4 the root within the circle outline (upper left corner) in each image. The N–S traverse images the E–W section of the root, whereas the E–W traverse images the N–S section. Combining both the N–S and E–W data sets provides a more complete image of the root. There is elongation of the imaging in the direction orthogonal to the survey direction; this is an artifact of the interpolation caused by the survey line spacing. The image quality could have been improved by

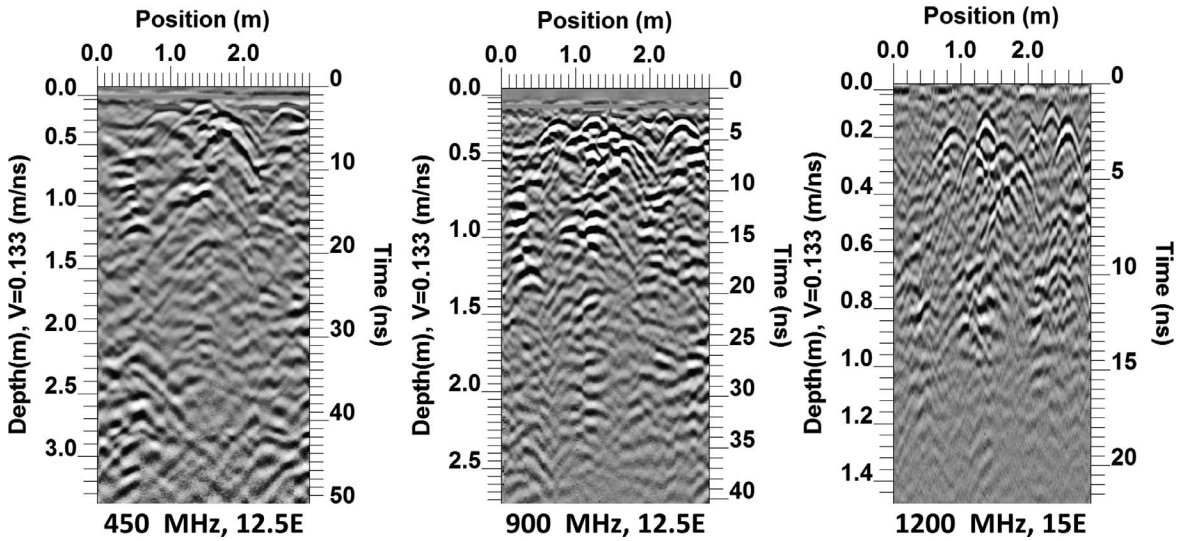

Figure 2. Comparison of GPR profiles acquired using different antenna frequencies along the same or adjacent lines. An EM wave velocity of V = 0.133 m/ns was used to estimate depth.

using a smaller line spacing. In the following discussion, only images of the combined 900 MHz data are presented, although final root delineations will be presented for each of the three antenna frequencies.

Depth slices such as those shown in Figs. 3 and 4 were used to physically map the roots identified in Fig. 5, which shows all roots mapped within the depth range 0–100 cm for each antenna frequency along with a combined map. The 450 MHz antenna detected the primary roots, while the 1200 MHz antenna provided additional detail on the shallower roots. As mentioned earlier, the collection of data in the E–W direction with the 900 MHz antenna imaged roots that were not detected using the other antennae, which were only operated in the N–S direction.

In Situ Root Measurement and Soil Analysis

Eleven roots greater than 2 cm in diameter were digitized. Each root was marked at 5-cm intervals for digitization unless an anomaly required greater resolution. Roots varied in length from 11 cm (Root 1A, 4 digitization points) to 247 cm (Root 4, 59 digitization points) and varied in maximum diameter from 2.27 cm (Root 6) to 8.02 cm (Root 4). Root diameter and digitization were used to estimate coarse root length and volume by assuming cylindrical root geometry. Table 1 presents measured coarse root volumes segregated by grid cell and depth interval.

Site-specific root densities were used to estimate fine root volume (Table 1). The total volume of roots (coarse + fine) decreases with distance away from the

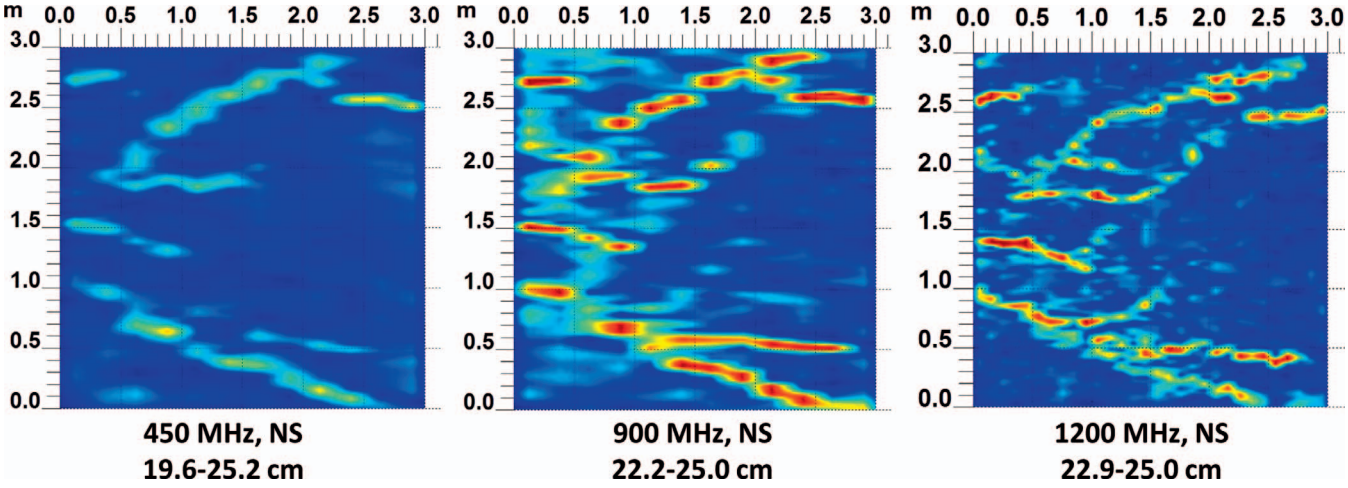

Figure 3. Comparison of GPR slices at similar depths for three antenna frequencies.

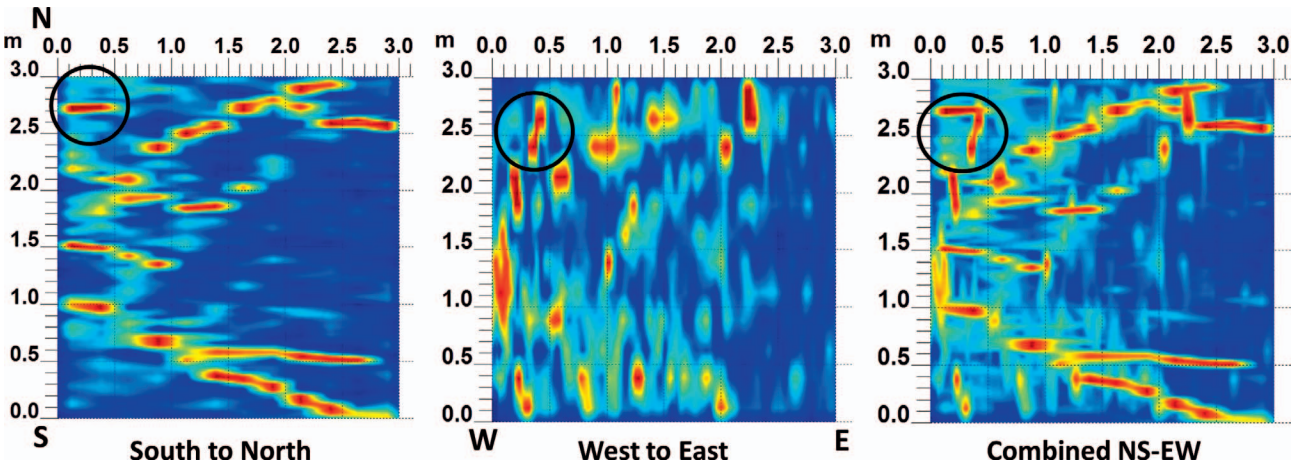

Figure 4. GPR data acquired using the 900 MHz antenna in both the N–S and E–W directions and the combined data set. Depth slice at 22 to 25 cm.

tree. Notably, the volume of fine and coarse roots is similar over the total sample area, 5973.5 cm^3 and 6245.0 cm^3, respectively. The majority of fine roots are found in the upper 50 cm (82% by volume), whereas the majority of coarse roots are in the 25–50 cm depth range (64% by volume).

Soil samples collected during root excavation were subjected to grain size, soil moisture and organic content analyses (Table 2). Grain size was uniform across each of the six cells, and the soil can be classified as medium to coarse sand (*e.g.*, for D_{50}, mean = 0.68 mm, standard deviation = 0.09, n = 24). Organic content was typically low (mean = 0.72%).

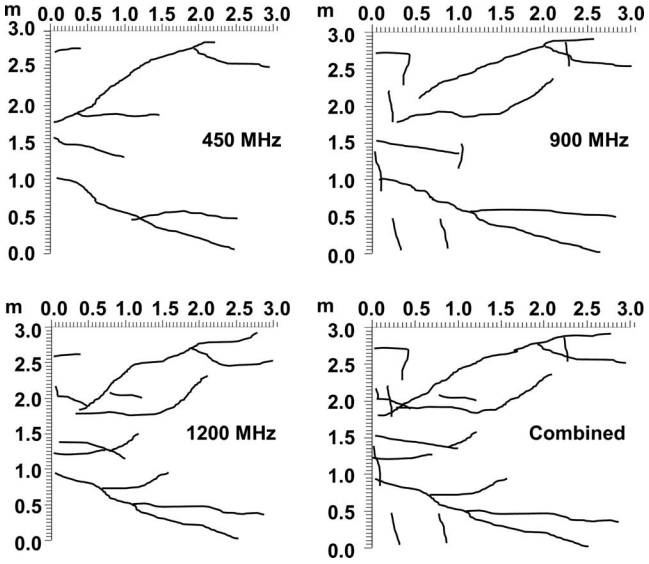

Figure 5. Root interpretation based on GPR depth slices for the individual frequencies and combined.

Discussion

A comparison of the GPR root location with the Polhemus digitized coarse root location is shown in Fig. 6. Of the coarse roots measured, the GPR location coincides with the actual root location, with the major discrepancy in the upper right (marked by the circle). Because the tree foliage interfered with use of a GPS, the GPR wheel odometer was used for all data positioning. The position mismatch could be attributed to an inconsistent walking speed and wheel odometer slippage while traversing the sand. The GPR was successful at imaging the larger roots (≥2 cm) and also mapped roots of lesser diameter. Images of the root volume determined from the GPR 9-m^2 surveyed area to a depth of 1 m using isovalues (point amplitudes, dimensionless) of 25000, 29150, and 30600 are shown in Fig. 7. The isovalue 25000 was chosen because it appears to represent the GPR combined image in Fig. 4, whereas the other two isovalues were selected because the 0–100 cm GPR root volumes are similar to the 0–100 cm in situ root volumes in cells A2 (isovalue 29150: GPR 4373 cm^3, in situ 4358 cm^3) and A3 (isovalue 30600: GPR 2376 cm^3, in situ 1938 cm^3). Selecting an isovalue that matches the GPR root volume to the in situ root volume provides local calibration, and a better fit between GPR and in situ results may be obtained. To compare the root volume determined by excavation to that determined using GPR, in the following discussion only the root volumes in the six excavated cells (Fig. 1) are used.

A comparison of the root volume from in situ measurement and GPR estimation for the six excavated cells is given in Table 3 and Fig. 8. For the depth range 0–100 cm, the total GPR root volume estimate is about

Table 1. Root volume estimates.

		Fine roots (<2 cm)		Coarse roots (>2 cm)		Total roots	
Cell	Depth (cm)	Mass (g)	Volume† (cm^3)	Mass* (g)	Volume‡ (cm^3)	Mass (g)	Volume (cm^3)
A1	0–25	272.4	486.5	0.0	0.0	272.4	486.5
	25–50	150.4	268.6	144.9	258.8	295.3	527.4
	50–75	84.7	151.3	1158.0	2067.8	1242.7	2219.1
	75–100	121.9	217.7	0.0	0.0	121.9	217.7
A2	0–25	392.5	700.9	55.2	98.5	447.7	799.4
	25–50	760.5	1358.1	1050.2	1875.3	1810.7	3233.4
	50–75	91.2	162.9	0.0	0.0	91.2	162.9
	75–100	91.0	162.5	0.0	0.0	91.0	162.5
A3	0–25	207.3	370.2	32.2	57.5	239.5	427.7
	25–50	194.1	346.6	547.8	978.3	741.9	1324.9
	50–75	24.6	43.9	0.0	0.0	24.6	43.9
	75–100	79.0	141.1	0.0	0.0	79.0	141.1
B2	0–25	279.5	499.1	0.0	0.0	279.5	499.1
	25–50	15.9	28.4	0.0	0.0	15.9	28.4
	50–75	18.5	33.0	0.0	0.0	18.5	33.0
	75–100	8.3	14.8	0.0	0.0	8.3	14.8
B3	0–25	234.7	419.1	10.8	19.2	245.5	438.3
	25–50	126.1	225.2	498.2	889.6	624.3	1114.8
	50–75	32.5	58.0	0.0	0.0	32.5	58.0
	75–100	37.8	67.5	0.0	0.0	37.8	67.5
C2	0–25	80.7	144.1	0.0	0.0	80.7	144.1
	25–50	33.1	59.1	0.0	0.0	33.1	59.1
	50–75	7.7	13.8	0.0	0.0	7.7	13.8
	75–100	0.6	1.1	0.0	0.0	0.6	1.1
All Cells	0–25	1467.1	2620.0	98.1	175.2	1565.2	2795.2
	25–50	1280.1	2286.0	2241.1	4002.0	3521.2	6288.0
	50–75	259.2	462.9	1158.0	2067.8	1417.2	2530.7
	75–100	338.6	604.7	0.0	0.0	338.6	604.7
	TOTAL	**3345.0**	**5973.5**	**3497.2**	**6245.0**	**6842.2**	**12,218.5**

† Estimated from mass (lab sample) and root density (0.560 g/cm^3).
* Estimated from volume (digitizer) and root density (0.560 g/cm^3).
‡ Estimated from digitizer measurements.

6, 1.5, and 0.73 times that of the total in situ root volume for isovalues 25000, 29150, and 30600, respectively (Table 3 bottom row, columns 4–6). Figures 8(a)–(c) compare in situ (fine, coarse, and total) and GPR root volumes for each of the excavated cells, which confirms the greatest discrepancy in the GPR volume estimate is obtained with isovalue 25000 (Fig. 8(a)) although this isovalue provided a visually comparable representation of the roots. Recall that isovalue 29150 was chosen for comparable root volumes in cell A2; therefore, in Fig. 8(b) there appears to be a single point for the total in situ and GPR volumes in cell A2; the same applies for isovalue 30600 and cell A1 in Fig. 8(c).

Figures 8(d)–(f) compare the total cell (0–100 cm) in situ root volume to the GPR estimate for the three isovalues. A linear fit and its R^2 value (square of the Pearson correlation coefficient) is given for each plot. Ideally, if there are no roots present in the subsurface, then the GPR should not detect any and, thus, the measured GPR root volume is zero. However, because of the presence of noise/clutter, it is possible that roots may be present and the GPR does not detect them. Likewise, the converse is possible, where the GPR interpretation identifies roots and none are present. A comparison of the calculated root volume using the three linear fits to the in situ root volume is given in Table 3. The measured GPR isovalue volumes in Table 3 (columns 4–6) were used in the respective linear fit equations (Figs. 8(d)–(f)) to obtain the calculated volumes (columns 7–9) for each isovalue. The higher R^2 value for isovalue 25000

Table 2. Summary of soil properties.

Cell	Depth (cm)	Organic content (%)	Moisture content† (%)	Grain size D_{90} (mm)	D_{50} (mm)	D_{10} (mm)
A1	0–25	1.45	2.82	4.21	0.50	0.26
	25–50	0.96	4.90	6.48	0.58	0.26
	50–75	0.36	4.04	>8	0.81	0.38
	75–100	0.98	6.51	4.75	0.62	0.29
A2	0–25	1.04	2.43	6.07	0.60	0.28
	25–50	0.48	3.84	6.64	0.72	0.30
	50–75	0.75	4.04	6.77	0.69	0.31
	75–100	0.64	3.97	6.86	0.69	0.32
A3	0–25	0.52	2.57	7.05	0.57	0.27
	25–50	0.34	3.44	7.22	0.60	0.26
	50–75	0.96	5.00	5.94	0.71	0.32
	75–100	0.36	4.40	4.26	0.65	0.28
B2	0–25	0.52	3.00	5.36	0.48	0.25
	25–50	2.06	3.37	>8	0.82	0.37
	50–75	1.05	5.14	6.17	0.75	0.37
	75–100	0.38	7.99	4.86	0.75	0.34
B3	0–25	0.59	2.30	6.33	0.69	0.30
	25–50	0.75	4.86	7.53	0.74	0.31
	50–75	0.26	4.75	6.88	0.72	0.34
	75–100	0.41	5.74	5.64	0.86	0.43
C2	0–25	1.34	3.00	7.32	0.64	0.28
	25–50	0.15	4.54	7.19	0.69	0.28
	50–75	0.66	5.17	6.52	0.71	0.32
	75–100	0.27	5.66	5.56	0.77	0.35

† Gravimetric moisture content.

suggests a better linear fit than the other isovalues, and the calculated volumes for the linear fit to isovalue 25000 are a better approximation to the in situ root volumes than achieved by the other isovalue linear fits. The differences in the total (0–100 cm) in situ root volume (Table 3 bottom row, column 3) and calculated root volume for isovalues 25000, 29150, and 30600 (Table 3 bottom row, columns 7–9) are 87 (0.7%), 339 (2.8%), and 468 (3.8%) cm^3, respectively. This suggests that matching the GPR root volume to a particular in situ root volume does not improve the root volume estimation.

In a practical field situation, if an area is going to be excavated to provide ground truth, it would be likely that only a few cells would be excavated to obtain near, intermediate, and far in situ root volume measurements. For the present study, cells A2, B2, and C2 represent a cell adjacent to the tree (A2) and at progressively greater distances along a straight line. A linear fit was applied to the measured in situ and GPR root volumes for cells A2, B2, and C2 (depth range 0–100 cm, isovalue 25000). A

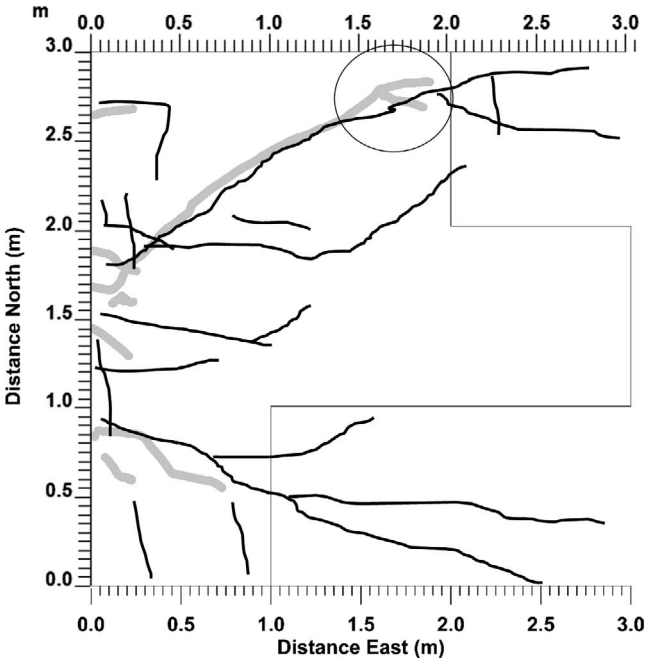

Figure 6. Combined GPR root interpretation (black lines) with Polhemus digitized root location (heavy gray lines) overlaid. The thin gray line represents the boundary of excavated cells.

comparison of the calculated root volumes to the in situ volumes based on this linear fit ($Y = 0.2131 \cdot X + 99.9$, $R^2 = 0.9984$) is provided in Table 4. The "Total" row represents the in situ root volume based on all six cells excavated (usually unknown), the GPR survey root volume estimate for the six cells excavated (known), and the calculated volume using the measured GPR volume as input to the three-cell linear fit. The total calculated volume (Table 4 bottom row, column 5) using only the three cells for the 0–100 cm depth range is 29.8% greater than the actual in situ volume (Table 4 bottom row, column 3). Considering the simplistic method used to estimate the tree root volume from the GPR data, an estimate within 30% of the actual in situ volume is adequate. It should be noted that the total calculated volume is estimated through extrapolation of the three-cell linear fit, which assumes the relationship between in situ and GPR root volume measurements is also linear at greater volumes. Figure 8(d), which is a plot of root volumes for all cells, confirms this linear relationship, at least for this tree.

The technique for estimating GPR root volume based on a selected amplitude response oversimplifies the problem and, in this case, resulted in an overestimation of the volume. However, depending on the purpose of a study, a rough estimate of the root volume may be acceptable, and the "visual volume mapping" approach

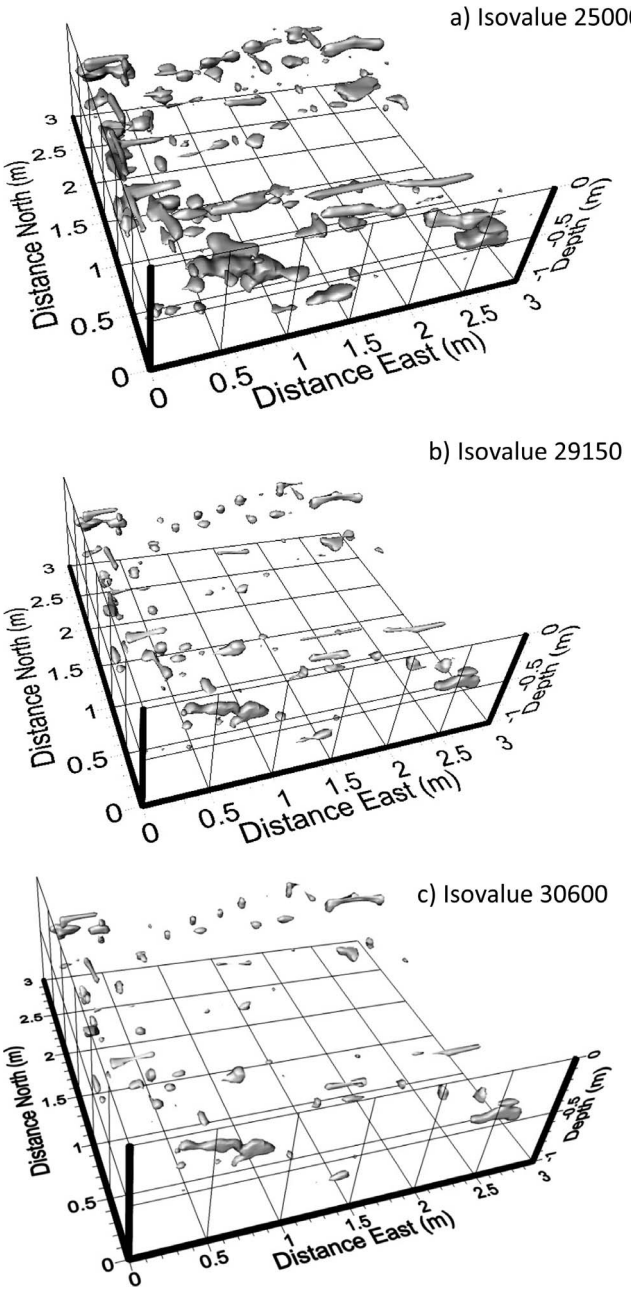

Figure 7. Images of root volume for depth interval 0–100 cm determined from the 900 MHz GPR survey for the entire 3-m×3-m grid. a) Isovalue 25000 that optimizes root visualization when compared with the combined 900-MHz GPR image in Fig. 4. b) Isovalue 29150 that gives a similar 0–100 cm GPR root volume (4373 cm^3) to the 0–100 cm in situ root volume (4358 cm^3) for cell A2. c) Isovalue 30600 that gives a similar 0–100 cm GPR root volume (2376 cm^3) to the 0–100 cm in situ root volume (1938 cm^3) for cell A3.

used to estimate the volume based on GPR data may suffice. Considering only the tree roots, the root volume estimate is dependent on how well the excavated areas represent the overall tree root volume. Roots are most commonly distributed close to a tree, and the selection of an area adjacent to the tree and areas progressively further away is a reasonable approach for selecting areas to excavate. The soil at this study site was a clean, well-sorted sand, which is probably atypical of soils encountered at other sites where root volume estimation may be of interest. For non-sandy soils, the background noise/clutter level will likely be higher, resulting in a greater discrepancy between the true and calculated root volume when using the proposed technique.

Conclusions and Opportunities for Future Research

This study assessed the feasibility of using ground penetrating radar to locate tree roots and estimate their subsurface volume. The clean, moist sand at this location provided a good environment (*i.e.*, low signal attenuation) for a GPR survey. The loblolly pine was well separated from other trees, so the major sources of subsurface anomalies were caused by roots of the selected tree. Roots smaller than 2-cm diameter were mapped. Use of orthogonally collected data sets provided a more complete image of the tree root system, and the position of the mapped roots agreed with excavation data. No attempt was made to estimate tree root diameter from the GPR data.

The estimated root volume based on GPR data was achieved through the selection of an isovalue that optimized the visual fit of the 3-D volume data presentation to the 2-D planar surfaces. A linear fit to the excavated root volume and GPR volume estimate was used to determine a calculated root volume. The calculated root volume was within 1% of the measured in situ root volume when information was used from all six of the excavated cells. When only three of the excavated cells were used, representing a near, intermediate, and far excavation sample, the difference between the in situ and calculated volume increased to 30%. It is possible that greater discrepancies could be obtained in different soil types and noisier data. A rough root volume estimate as obtained from this simplistic volume estimation technique based on GPR data may be suitable depending on its purpose and application.

The following topics highlight potential areas of future research related to in situ detection, measurement, and volume estimation of roots.

Table 3. Measured root volume from GPR (900 MHz) and in situ sampling. Calculated root volumes are based on linear fits to all excavated cells for depth range 0–100 cm.

		Measured root volume (cm^3)				Calculated root volume (cm^3)		
			GPR isovalue			GPR isovalue		
Cell	Depth (cm)	In situ	25000	29150	30600	25000	29150	30600
A1	0–50	1014	10,009	3021	1405	1671	2021	2023
	50–100	2437	13,593	3988	2046	2258	2625	2860
	0–100	3451	23,602	7008	3451	3895	4510	4695
A2	0–50	4033	13,393	3279	1459	2225	570	273
	50–100	325	7137	1094	464	1201	213	110
	0–100	4358	20,530	4373	1923	3393	2865	2699
A3	0–50	1753	12,166	4031	2098	2024	693	377
	50–100	185	5297	791	279	900	163	79
	0–100	1938	17,463	4822	2376	2891	3146	3291
B2	0–50	528	859	160	38	174	60	40
	50–100	48	1031	90	23	203	49	38
	0–100	575	1891	250	61	343	292	267
B3	0–50	1553	7123	1793	829	1199	327	169
	50–100	126	2524	491	198	447	114	66
	0–100	1679	9646	2283	1026	1612	1561	1528
C2	0–50	203	243	15	2	74	36	34
	50–100	15	567	63	13	127	44	36
	0–100	218	811	78	14	167	184	206
Total	0–50	9083	43,793	12,298	5830	7198	7812	7803
	50–100	3135	30,149	6516	3022	4966	4203	4135
	0–100	12,218	73,942	18,814	8852	12,131	11,879	11,750

- *Application to other environments*: This method should be applied to different soil types and tree types, which could introduce greater challenges for root detection. Questions regarding the feasibility of the proposed technique in other environments and if relationships exist for estimating root volume in different environments should be addressed.
- *Quantitative validation*: This comparison between GPR predictions and excavated root morphology has been primarily qualitative in nature. Quantitative comparisons among root detection methods should be conducted to determine the strengths and limitations of the techniques. Key topics to be addressed include detection thresholds in root size, soil type, and depth, application of spatial statistics to examine the accuracy of root predictions with respect to location and orientation, and the capacity to predict bulk properties.
- *Increasing reflected signal strength*: This study has examined a single tree in a favorable soil environment. The soil conditions suitable for GPR are relatively well-known (Doolittle *et al*., 2007). However, the interaction between soil and plant conditions has not been adequately addressed. For instance, taxa with greater wood density (*i.e*., higher specific gravity) may provide a stronger contrast between soil and roots, and thus a better prediction of root morphology (Butnor *et al*., 2001). Additionally, there may be techniques for increasing the reflected signal strength by modifying the root environment with moisture or injecting an electrical current into the roots. Because the tree trunk and root system do contain moisture, it may be possible to inject a current into the tree at the base of the trunk which could flow into the roots. The GPR may be able to detect the weak currents flowing in the roots.
- *Root volume from GPR measurements vs. root ball volume*: The relationship between root volume estimates from GPR measurements and root ball volume estimates obtained from empirical correlations or estimates from electrical resistivity tomography (ERT) should be studied.
- *GPR modeling*: Forward modeling the GPR response of roots to include variations in soil properties (soil type, electrical conductivity and relative dielectric permittivity) and root properties (tree type, relative

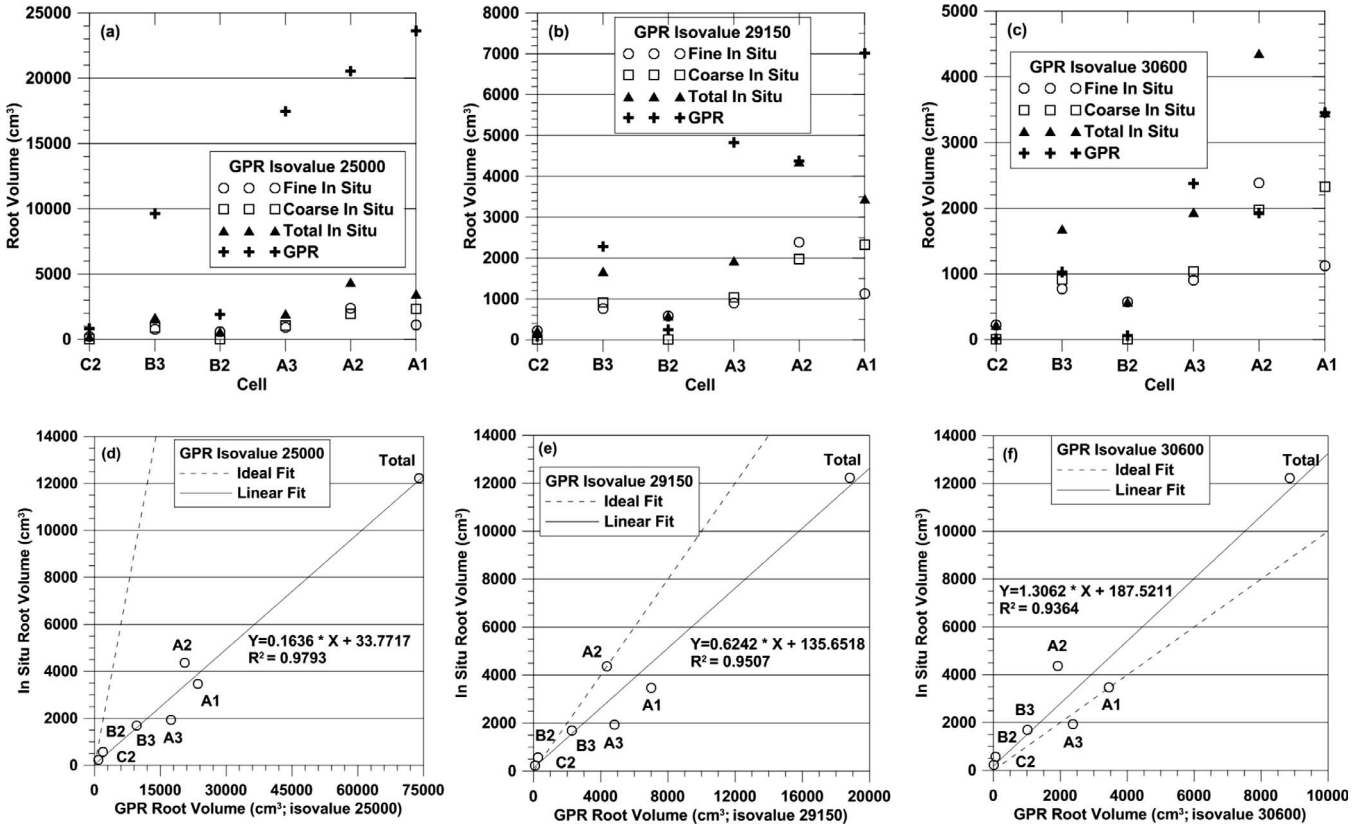

Figure 8. Comparison of root volumes determined from in situ measurement and GPR estimates for 0–100 cm depth. Volume is in units of cm^3. (a)–(c) are root volumes within each cell for isovalues 25000, 29150, and 30600, respectively. (d)–(f) are in situ root volume vs. GPR root volume for isovalues 25000, 29150, and 30600, respectively. The point labels correspond to the cells and total volume. The equation is a linear fit.

Table 4. Comparison of root volumes for in situ, GPR, and calculated based on the linear fit to excavated cells A2, B2, and C2 for depth range 0–100 cm. Linear fit equation ($Y = 0.2131 \cdot X + 99.9$, $R^2 = 0.9984$).

		Measured volume (cm^3)		Calculated volume from linear fit (cm^3)
Cell	Depth (cm)	In situ	GPR isovalue 25000	GPR isovalue 25000
A2	0–50	4033	13,393	2955
	50–100	325	7137	1622
	0–100	4358	20,530	4477
B2	0–50	528	859	283
	50–100	48	1031	320
	0–100	575	1891	503
C2	0–50	203	243	152
	50–100	15	567	221
	0–100	218	811	273
Total All Cells	0–50	9083	43,793	9437
	50–100	3135	30,149	6528
	0–100	12,218	73,942	15,864

dielectric permittivity and root dimensions) to aid in determining subsurface conditions in which GPR imaging would be most successful. Modeling may also be useful for estimating root size by correlating GPR imaging with modeling results.

Acknowledgments

The authors gratefully acknowledge the laboratory and field assistance provided by Albert Winschel. Site access was provided by James Marble on behalf of Vicksburg Sand and Gravel. This work was funded under an investigation of the "Initial Research into the Effects of Woody Vegetation on Levees" (Corcoran *et al*., 2011) by Headquarters, U.S. Army Corps of Engineers, Flood & Coastal Storm Damage Reduction Program. Permission to publish was granted by Director, Geotechnical and Structures Laboratory.

References

Barton, C.V.M., and Montagu, K.D., 2004, Detection of tree roots and determination of root diameters by ground penetrating radar under optimal conditions: Tree Physiology, **24**, 1323–1331.

Butnor, J.R., Doolittle, J.A., Kress, L., Cohen, S., and Johnsen, K.H., 2001, Use of ground-penetrating radar to study tree roots in the southeastern United States: Tree Physiology, **21**, 1269–1278.

Butnor, J.R., Doolittle, J.A., Johnsen, K.H., Samuelson, L., Stokes, T., and Kress, L., 2003, Utility of ground-penetrating radar as a root biomass survey tool in forest systems: Soil Science Society of America Journal, **67**, 1607–1615.

Butnor, J.R., Stover, D.B., Roth, B.E., Johensen, K.H., Day, F.P., and McInnis, D., 2008, Using ground-penetrating radar to estimate tree root mass comparing results from two Florida surveys: *in* Handbook of Agricultural Geophysics, Allred, B.J., Daniels, J.J., and Ehsani, M.R. (eds.), CRC Press, Boca Raton, 375–382.

Cermak, J., Neruda, J., Nadezdina, N., Ulrich, R., Martinkova, M., Gebauer, R., Pokorny, E., Nadezdin, V., Hruska, J., Gasparek, J., and Culek, I., 2006, Identification of tree root system damage caused by heavy machinery using new measurement technology suitable for precision forestry: *in* Proceedings of the International Precision Forestry Symposium, Stellenbosch University, South Africa, 291–304.

Corcoran, M.K., Peters, J.F., Dunbar, J.B., Llopis, J.L., Tracey, F.T., Wibowo, J.L., Simms, J.E., Kees, C.E., McKay, S.K., Fischenich, J.C., Farthing, M.W., Glynn, M.E., Robbins, B.A., Strange, R.C., Schultz, M.T., Clarke, J.U., Berry, T.E., Little., C.D. and Lee, L.T., 2011, Initial research into the effects of woody vegetation on levees, Technical Report ERDC TR to HQUSACE, U.S. Army Engineer Research and Development Center, Vicksburg, MS.

Cui, XH., Chen, J., Shen, JS., Cao, X., Chen, XH., and Zhu, XL., 2011, Modeling tree root diameter and biomass by ground-penetrating radar: Science China Earth Sciences, **54**, 711–719.

Cui, X., Guo, L., Chen, J., Chen, X., and Zhu, X., 2013, Estimating tree-root biomass in different depths using ground-penetrating radar: Evidence from a controlled experiment: IEEE Transactions on Geoscience and Remote Sensing, **51**, 3410–3423.

Danjon, F., Barker, D.H., Drexhage, M., and Stokes, A., 2008, Using three-dimensional plant root architecture in models of shallow-slope stability: Annals of Botany, **101**, 1281–1293.

Danjon, F., and Reubens, B., 2008, Assessing and analyzing 3D architecture of woody root systems, a review of methods and applications in tree and soil stability, resource acquisition and allocation: Plant and Soil, **303**, 1–34.

Danjon, F., Caplan, J.S., Fortin, M., and Meredieu, C., 2013, Descendant root volume varies as a function of root type: Estimation of root biomass lost during uprooting in *Pinus pinaster*: Frontiers in Plant Science, **4**, Article 402, 1–16.

Day, S.D., Wiseman, P.E., Dickinson, S.B., and Harris, J.R., 2010, Tree root ecology in the urban environment and implications for a sustainable rhizosphere: Arboriculture & Urban Forestry, **36**, 193–205.

Di Iorio, A., Lasserre, B., Scippa, G.S., and Chiatante, D., 2005, Root system architecture of *Quercus pubescens* trees growing on different sloping conditions: Annals of Botany, **95**, 351–361.

Doolittle, J.A., Minzenmayer, F.E., Waltman, S.W., Benham, E.C., Tuttle, J.W., and Peaslee, S.D., 2007, Ground-penetrating radar soil suitability map of the conterminous United States: Geoderma, **141**, 416–421.

Freeland, R.S., 2015, Imaging the lateral roots of the orange tree using three-dimensional GPR: Journal of Environmental and Engineering Geophysics, **20**, 235–244.

Guo, L., Chen, J., Cui, X., Fan, B., and Lin, H., 2013a, Application of ground penetrating radar for coarse root detection and quantification: A review: Plant Soil, **362**, 1–23.

Guo, L., Lin, H., Fan, B., Cui, X., and Chen, J., 2013b, Impact of root water content on root biomass estimation using ground penetrating radar: Evidence from forward simulations and field controlled experiments: Plant Soil, **371**, 503–520.

Hirano, Y., Dannoura, M., Aono, K., Igarashi, T., Ishii, M., Yamase, K., Makita, N., and Kanazawa, Y., 2009, Limiting factors in the detection of tree roots using ground-penetrating radar: Plant Soil, **319**, 15.

Hruska, J., Cermak, J., and Sustek, S., 1999, Mapping tree root systems with ground-penetrating radar: Tree Physiology, **19**, 125–130.

Nadezhdina, N., and Cermak, J., 2003, Instrumental methods for studies of structure and function of root systems of large trees: Journal of Experimental Botany, **54**, 1511–1521.

Randrup, T.B., McPherson, E.G., and Costello, L.R., 2001, Tree root intrusion in sewer systems: Review of extent and costs: Journal of Infrastructure Systems, **7**, 26–31.

Schroeder, K., 2005, Konkurrenz unter Tage [Competition underground]: GrenForum.LA, **4**, 34–38.

Stokes, A., Fourcaud, T., Hruska, J., Cermak, J., Nadyezdhina, N., Nadyezhdin, V., and Praus, L., 2002, An evaluation of different methods to investigate root system architecture of

urban tress in situ: I. Ground-penetrating radar: Journal of Arboriculture, **28**, 2–10.

Yeung, S.W., Yan, W.M., and Hau, C.H.B., 2016, Performance of ground penetrating radar in root detection and its application in root diameter estimation under controlled conditions: Science China Earth Sciences, **59**, 145–155.

Yokota, Y., Matsumoto, M., Gaber, A., Grasmueck, M., and Sato, M., 2011, Estimation of biomass of tree roots by GPR with high accuracy positioning system: IEEE International Geoscience and Remote Sensing Symposium (IGARSS), 190–193.

Zanetti, C., Weller, A., Vennetier, M., and Meriaux, P., 2011, Detection of buried tree root samples by using geoelectrical measurements: A laboratory experiment: Plant and Soil, **339**, 273–283.

Zhu, S., Huang, C., Su, Y., and Sato, M., 2014, 3D ground penetrating radar to detect tree roots and estimate root biomass in the field: Remote Sensing, **6**, 5754–5773.